Chinese Chemical Letters 36 (2025) 109988

Contents lists available at ScienceDirect

Chinese Chemical Letters

journal homepage: www.elsevier.com/locate/cclet

Flexible aqueous zinc-ion battery with low-temperature resistant leather gel electrolyte

Mengxiao Yang[a], Haicheng Huang[a], Shiyi Shen[b], Xinxin Liu[a], Mengyu Liu[b], Jiahua Guo[b], Fenghui Yang[a], Baoli Zha[a], Jiansheng Wu[a,*], Sheng Li[a,*], Fengwei Huo[a]

[a] Key Laboratory of Flexible Electronics (KLOFE), School of Flexible Electronics (Future Technologies), Institute of Advanced Materials (IAM), Nanjing Tech University, Nanjing 211816, China
[b] School of Chemistry and Molecular Engineering, Nanjing Tech University, Nanjing 211816, China

ARTICLE INFO

Article history:
Received 29 February 2024
Revised 3 April 2024
Accepted 9 May 2024
Available online 10 May 2024

Keywords:
Flexible zinc ion batteries
Leather
Gel electrolyte
Hydrogen bonding acceptor

ABSTRACT

Flexible zinc-ion batteries (FZIBs) have been acknowledged as a potential cornerstone for the future development of flexible energy storage, yet conventional FZIBs still encounter challenges, particularly concerning performance failure at low temperatures. To address these challenges, a novel anti-freezing leather gel electrolyte (AFLGE-30) is designed, incorporating ethanol as a hydrogen bonding acceptor. The AFLGE-30 demonstrates exceptional frost resistance while maintaining favorable flexibility even at −30 °C; accordingly, the battery can achieve a high specific capacity of about 70 mAh/g. Cu//Zn battery exhibits remarkable stability at room temperature, retaining ~96% efficiency after 120 plating/stripping cycles at 1 mA/cm^2. Concurrently, the Zn//Zn symmetric batteries demonstrate a lifespan of 4100 h at room temperature, which is attributed to the enhancement of Zn^{2+} deposition kinetics, restraining the formation of zinc dendrites. Furthermore, FZIBs exhibit minimal capacity loss even after bending, impacting, or burning. This work provides a promising strategy for designing low-temperature-resistant FZIBs.

With the rapid development of smart clothing, implantable medical devices, artificial electronic skin, and other flexible wearable electronic devices, the demand for energy storage devices is escalating [1,2]. Flexible zinc-ion batteries (FZIBs) are regarded as promising energy storage solutions, propelling the progress of emerging wearable electronic devices owing to their low redox potential (−0.76 V), substantial theoretical specific capacity (820 mAh/g), enhanced safety, and cost-effectiveness [3-6]. However, FZIBs based on conventional liquid electrolytes may suffer from electrolyte leakage, leading to rapid device failure [7,8]. *Quasi*-solid gel electrolytes, characterized by a distinctive three-dimensional (3D) network structure and excellent flexibility, have proven to be a suitable electrolyte choice for FZIBs [9-12]. In nature, the skin of many plants and animals, including cow leather, can resist damage from low temperatures [13]. A large number of collagen fibers in cow leather intertwine with each other to form collagen fiber clusters, giving it good mechanical strength [14]. In addition, cow leather possesses good ionic transport properties, making it an excellent material for *quasi*-solid gel electrolytes [15-17].

However, a significant challenge for FZIBs lies in the electrolyte freezing at low temperatures, leading to reduced ionic transport and destabilization of zinc metal through dendrite growth [18]. The freezing process of water involves organizing disordered water molecules into an ordered lattice of ice crystals through intermolecular hydrogen bonding (H-) [19,20]. Accordingly, breaking these hydrogen bonds is key to lowering the freezing point of the hydrogel electrolyte [21]. In addition, zinc nucleation in the electrolyte will trigger substantial dendrite growth. The cycling-induced reduction of H^+ results in the production of hydrogen gas, accompanied by the formation of the insoluble by-product $Zn_4SO_4(OH)_6$-xH_2O. This process leads to the deactivation of the zinc surface and hinders its embedding/de-embedding [22,23]. Thus, it is still crucial to optimize the interface between the gel electrolyte and the zinc anode to inhibit the formation of zinc dendrites [24].

Various strategies have been tried to solve the problem of electrolyte icing, including the formation of highly concentrated electrolytes, the introduction of ionic liquids, and the utilization of organic additives [25-27]. For example, dimethyl sulfoxide (DMSO), acetonitrile (AN), and glycerol (GI) have been used as organic additives to formulate co-solvents with H_2O in order to lower the freezing point of electrolytes [28-30]. Researchers used ethylene

* Corresponding authors.
E-mail addresses: iamjswu@njtech.edu.cn (J. Wu), iamsli@njtech.edu.cn (S. Li).

https://doi.org/10.1016/j.cclet.2024.109988
1001-8417/

glycol (EG) as an organic additive to effectively enhance the hydrogen bonding with H_2O and weaken the solubilization of Zn^{2+} with H_2O, thus lowering the freezing point of the solution [31,32]. Huang *et al.* designed a functional 3D network hydrogel electrolyte (PDC-20) lined with hydrogen bonding receptors, which improved the mechanical properties of the hydrogel electrolyte while lowering the freezing point due to breaking the hydrogen bonds in H_2O [20]. Despite significant progress, the low-temperature performance of zinc batteries is still far from satisfactory. However, compared with this type of organic solvent, ethanol has a lower freezing point, which is −114.2 °C. In addition, viscous antifreezes such as glycerol have high density, high viscosity, and poor fluidity, which can easily lead to low ion transmission rates of electrolytes when used as antifreezes [33,34]. As we know, ethanol, as a non-polar solvent, can form strong hydrogen bonds with H_2O, destroying the original hydrogen bonding structure between water molecules. So far, there is limited research on the modulation of low-temperature resistance of hydrogel electrolytes using ethanol in ZIBs. Moreover, the effect of ethanol on the mechanical properties of hydrogel electrolytes and hydrogel solvation has not been systematically studied.

Here, we prepared an anti-freezing leather gel electrolyte (AFLGE) consisting of leather fibers, $Zn(OTF)_2$ solution and ethanol (EtOH). AFLGE exhibits robust mechanical characteristics while demonstrating superior electrochemical performance at −30 °C compared to traditional aqueous electrolytes. The leather gel, employed as the matrix material in AFLGE, exhibits commendable mechanical properties and a substantial presence of hydrophilic groups, including hydroxyl and carboxyl groups. This composition is advantageous for augmenting the H_2O content of the electrolyte and enhancing its tolerance to electrolyte salts. Ternary hydrogen bonding (HB) interactions between the hydrogen bonding acceptor EtOH, H_2O, and polymer chains are observed to decrease the activity of H_2O, effectively lowering the freezing point of the AFLGE. Furthermore, EtOH molecules play a role in the solvation structure of Zn^{2+} prior to H_2O, contributing to the optimization of Zn^{2+} deposition kinetics and the inhibition of dendrite growth and side reactions of Zn. The Cu//Zn battery utilizing anti-freezing leather gel electrolyte-30% (AFLGE-30) demonstrates remarkable stability, retaining approximately 96% efficiency after 120 plating/stripping cycles at 1 mA/cm^2. Moreover, the Zn//Zn symmetric battery exhibits an extended operational life of up to 4100 h. The FZIBs assembled with AFLGE-30 demonstrate the capability to sustain a specific capacity of 70 mAh/g at a current density of 100 mA/g, even under low-temperature conditions of −30 °C. Additionally, FZIB systems exhibit negligible capacity loss even after undergoing bending, pounding, and burning, demonstrating resilience under harsh conditions.

The preparation process of AFLGE-30 is illustrated in Fig. 1a. The leather, produced through a tanning process, retains its collagen fiber structure in the raw cowhide, enhancing collagen fiber dispersion and porosity. The simulated effects of ethanol addition on the molecules and ions within the $Zn(OTF)_2$ solution are illustrated in Fig. 1b. Ethanol molecules replace water molecules and anions around zinc ions in the solution, thus weakening the interaction between zinc ions and water molecules. Moreover, ethanol's freezing point of −114.2 °C in the standard state indicates better freezing resistance (Fig. S1 in Supporting information), thereby affecting the physical and chemical properties of the solution.

AFLGE-30 remains flexible when twisted in the temperature range of 25 °C to −40 °C, and the liquid electrolyte containing 30% EtOH shows no signs of icing (Fig. 1c). Scanning electron microscopy (SEM) image reveals that AFLGE-30 has a unique pore structure that facilitates the accommodation and transport of ions, possibly due to the increased porosity and the relaxation of intercollagen binding that occur after the gelation process (Fig. 1d).

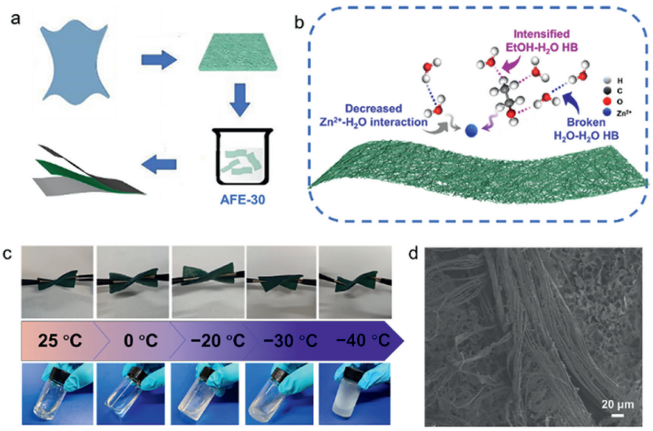

Fig. 1. (a) Fabrication procedure for AFLGE-30 gel electrolyte. (b) Simulation study on the molecular and ionic effects of ethanol addition in $Zn(OTF)_2$ solution. (c) Physicochemical characteristics of AFLGE-30 gel electrolyte and liquid electrolyte with 30% EtOH added in the temperature range from 25 °C to −40 °C. (d) SEM image of AFLGE-30 gel electrolyte.

It is noteworthy that, the characteristic Fourier transform infrared peaks of the gelatinized leather are similar to those of the chrome-tanned leather (S2), which indicates that no damage to its functional groups after gelatinization [35,36].

Due to the large number of complex groups in leather, a liquid solution is used as the electrolyte for testing to prevent any interference from the leather with the test results. Co-solvents with diverse concentrations are generated by adjusting the ratio of electrolyte to ethanol, leading to corresponding modifications in both physical and chemical properties. The co-solvents with 0%, 10%, 15%, 20%, 25%, and 30% ethanol content were named AFE-0, AFE-10, AFE-15, AFE-20, AFE-25, and AFE-30, respectively. To elucidate the interaction of ethanol in antifreeze gel electrolytes, Raman and ^{1}H nuclear magnetic resonance tests are performed on electrolytes containing -H and -OH groups. Figs. 2a and b show the Raman spectra of mixed electrolytes with different ethanol ratios. A unique -OH stretching vibration peak is shown at approximately 3400 cm^{-1}, blue-shifting with increasing ethanol content, likely due to the formation of a more stable hydrogen bonding group between -OH in ethanol and -H in water [37]. This result is similar to the Raman characteristic curve in the H_2O-ethanol co-solvent system (Fig. S3 in Supporting information). To further confirm hydrogen bond formation and vibrational shifts resulting from solvation between Zn^{2+} and ethanol, NMR detection is employed. With an increase in ethanol content, a downfield shift in the chemical shift of the proton is observed, which signifies a reduction in the electron cloud density around H, resulting in an enhanced deshielding effect and increased propensity for hydrogen bond formation (Fig. 2c). Similarly, the ^{1}H NMR curve of the co-solvent comprising H_2O and ethanol (Fig. S4 in Supporting information) reveals a lower field shift in the chemical shift of the proton. Furthermore, the hydrogen bond contents of antifreeze gel electrolytes AFLGE-15, AFLGE-20, AFLGE-25, and AFLGE-30 are assessed using nuclear magnetic resonance (Fig. 2d). Wherein, AFLGE-15, AFLGE-20, AFLGE-25, and AFLGE-30 refer to leather gel electrolytes with 15%, 20%, 25%, and 30% ethanol content, respectively. The findings indicate that, similar to the earlier conclusion, an increase in ethanol content corresponds to a shift towards a lower field in the nuclear magnetic resonance curve of the antifreeze gel electrolyte. The freezing point of the antifreeze gel electrolyte is also tested by differential scanning calorimetry in order to further demonstrate the performance of AFLGE-30 gel electrolyte at low temperatures (Fig. 2e). No freezing occurs in AFLGE-30 in the temperature range of −70∼25 °C, while a change in the composition of the elec-

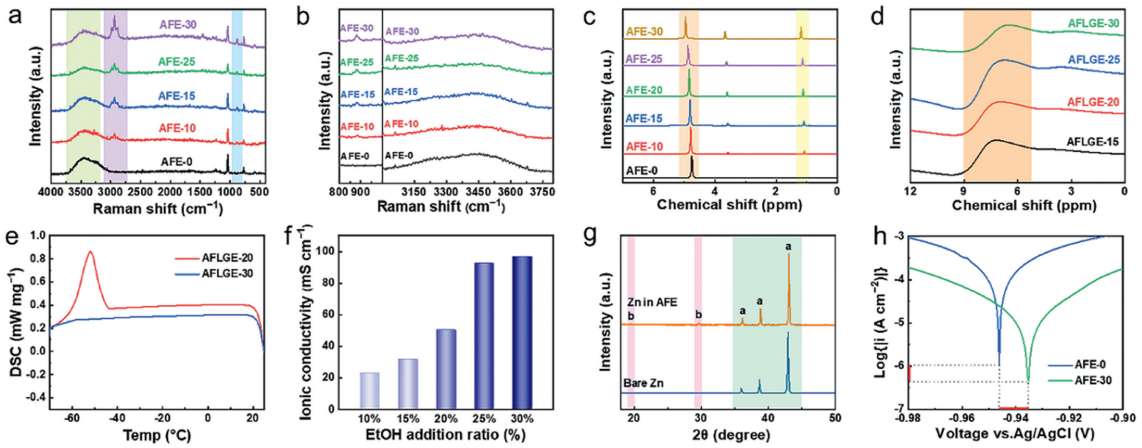

Fig. 2. (a) Raman curves (b) -OH stretching vibrational peaks of electrolytes containing different proportions of ethanol. ^{1}H nuclear magnetic resonance spectra of (c) liquid electrolytes and (d) gel electrolytes with different ethanol additions. (e) DSC curves of AFLGE-20 and AFLGE-30. (f) Ionic conductivity at −30 °C for gel electrolytes with different ethanol contents. (g) XRD curves of zinc foils after immersion in AFE-30 electrolyte for seven days. (h) The corrosion potential of the electrolyte is evaluated in AFLGE-30 electrolyte utilizing a three-electrode system.

trolyte may lead to a gradual increase in the radius of the dissolved structure of Zn^{2+}, which may result in a higher ionic conductivity than that of a leather gel electrolyte with an ethanol content of 10%−25% (Fig. 2f) [20,38,39].

To investigate the performance of the AFE-30 solution in protecting the zinc anode, zinc foil is analysed by X-ray diffraction after being immersed in AFE-30 electrolyte for seven days (Fig. 2g). Two additional diffraction peaks are observed in the zinc foil post-immersion as compared to the zinc foil pre-immersion in region b which indicates the development of a passivation layer on its surface. In a three-electrode system, linear polarization tests are conducted to investigate the corrosion behavior of zinc foil in various electrolytes. Notably, the corrosion potential of zinc in the AFE-30 solution exhibits a significant increase and the corrosion current density is lower (Fig. 2h). These observations highlight the effectiveness of the AFE-30 solution in decelerating the corrosion rate of zinc foil within the electrolyte. The consistency of these results with our earlier XRD tests reinforces the reliability of the findings.

The deposition behaviors of zinc ions in AFE-0 solution and AFE-30 solution under high current density (10.0 mA/cm^2) are observed through *in situ* optical microscopy (Fig. 3a). After 20 min, a clear shadow appears on the surface of the zinc foil, which indicates the formation of zinc dendrites. The zinc dendrites will grow and aggregate over time, potentially penetrating the separator and causing a short circuit in the battery. In contrast, no noticeable zinc dendrites are observed on the surface of zinc even after 60 min of deposition in the AFE-30 solution. The uniform deposition of zinc in the AFE-30 solution, which impedes the growth of zinc dendrites, signifies an effective enhancement in the protective capability of the zinc anode within the battery.

Zinc dendrites and passivation layers are formed during charging and discharging and are aggregated in a spherical shape [40]. Subsequently, coin batteries are used to demonstrate that AFLGE-30 has a better protective effect on the zinc electrodes than that based on the liquid electrolyte. After 20 cycles at a current density of 2 mA/cm^2, no discernible zinc dendrites are observed on the surface of the zinc foil, and the passivation layer has not yet fully developed (Fig. S5a in Supporting information). After 50 cycles (Fig. S5b in Supporting information), the number of spherical dendrites increases, with a small number of dendrites also present on the collagen fibers. As the number of circulating laps increases, the number of residual collagen fibers and the tendency of dendrite growth on collagen fibers increase as well (Fig. S5c in Supporting information). Fig. 3b shows a typical SEM image of zinc electrode after the Zn stripping/plating at 2 mA/cm^2 for 200 cycles, where the dendrites basically grow on the collagen fibers, whereas the passivation layer on the surface of the zinc foil is relatively smooth. This indicates that collagen fibers gradually become an important growth point for dendrites [41].

The passivation layer appears on the surface of the Zn anode using AFLGE-30 (Fig. S6a in Supporting information). After 200 cycles, the passivation layer on the Zn anode still behaves smoothly, and no dendrites (leather fibers in the form of threads) are formed on the surface (Fig. 3c). In contrast, the zinc anode with AFE-0 solution loses its metallic luster on the surface after 20 cycles, and the zinc dendrites aggregate from the periphery to the center and become tightly bound to the surface of the zinc foil after 200 cycles (Fig. S6 in Supporting information) [42]. Cu//Zn coin battery is assembled to evaluate the reversibility of electroplating/stripping of Zn^{2+} to be around 96% after 120 cycles at a current density of 1 mA/cm^2 (Fig. 3d). The capacity-voltage curves in the 10th, 50th and 100th cycles are selected to further observe the capacity-voltage of the battery (Fig. 3e). It is observed that the voltage difference of the FZIB using AFLGE-30 remains small after a long cycling period, demonstrating the excellent plating/stripping reversibility of zinc with the AFLGE-30. To demonstrate the long-cycle performance of the AFLGE-30, the Zn//Zn symmetric batteries assembled with AFE-30 and AFLGE-30 are subjected to constant-current charge/discharge tests at a current density of 1 mA/cm^2 (Fig. 3f). Table S1 (Supporting information) shows a comparison of the plating stripping life of Zn//Zn symmetric batteries assembled with AFLGE-30 and other electrolytes [43-47]. Compared to most of the reported electrolytes, AFLGE-30 exhibits an excellent electroplating stripping life of 4100 h at 1 mA/cm^2. However, while the symmetric battery using AFLGE-30 has a longer life, it has a larger voltage hysteresis compared to using glass fiber as a diaphragm, which may be caused by the much lower ionic conductivity of the AFLGE-30 than that of the liquid electrolyte. Moreover, the AFLGE-30 is much thicker (1.6 mm) than glass fiber (0.2 mm), likely resulting in a symmetric battery with a larger voltage hysteresis and greater resistance (Fig. S7 in Supporting information).

Subsequently, full batteries are assembled using FeV_3O_9 as the cathode material to further evaluate the electrochemical performance of AFLGE-30. EIS testing of coin batteries using AFLGE-15, 20, 25 and 30 are conducted at −30 °C to validate the effectiveness of the AFLGE-30 at low-temperature. The AFLGE-30 battery exhibits the smallest charge transfer resistance (Fig. 4a). However, the ion mobility in the gel electrolyte decreases with the rise in

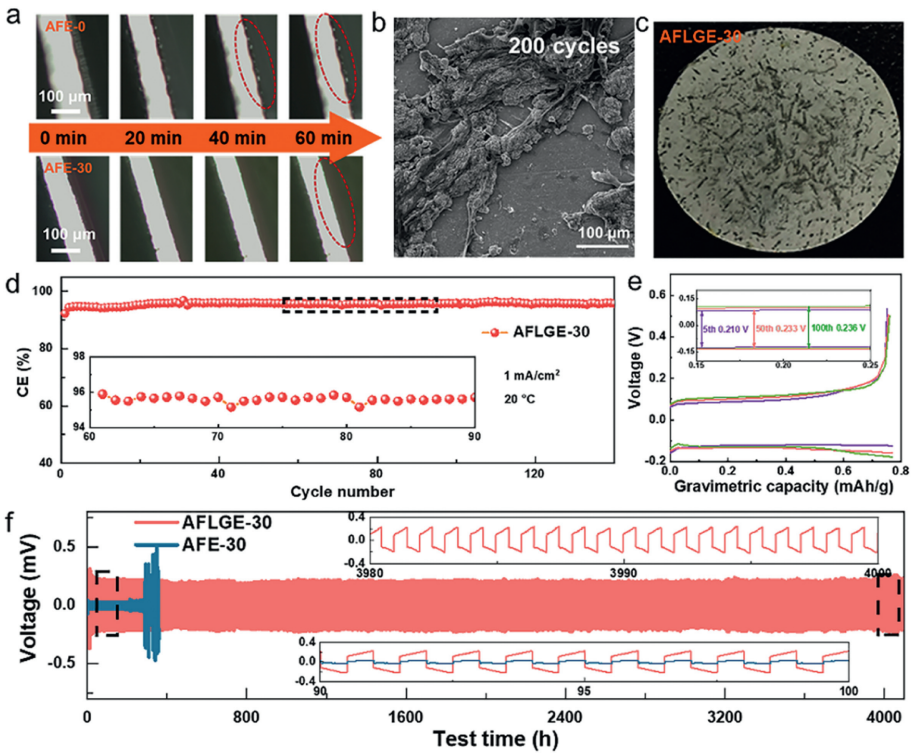

Fig. 3. (a) *In-situ* optical microscope observation of the deposition behavior of zinc foil in AFE-0 and AFE-30 liquid electrolytes. (b, c) SEM and optical pictures of AFLGE-30 assembled Zn//Zn symmetric after 200 cycles. (d) Coulombic efficiency of AFLGE-30 assembled Cu//Zn batteries. (e) Capacity-voltage profile during charging and discharging. (f) Long cycle performance of Zn//Zn symmetric batteries assembled with AFLGE-30 and AFE-30 liquid electrolytes.

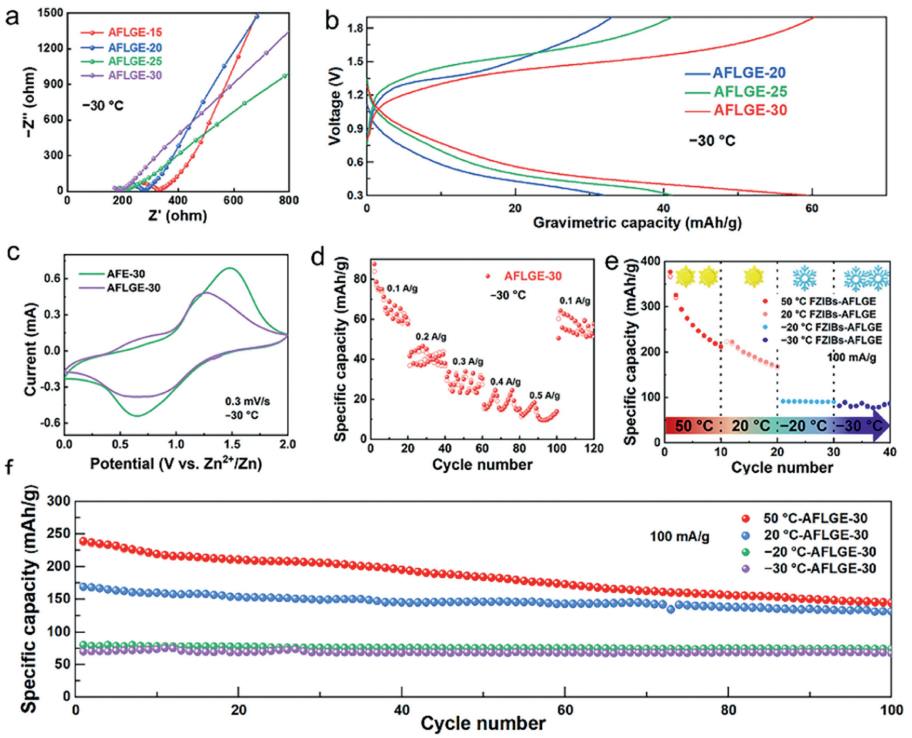

Fig. 4. (a) EIS testing of coin batteries using AFLGE-15, 20, 25 and 30 at −30 °C. (b) Charge-discharge curves of FZIB using AFLGE-20, 25, 30 at −30 °C. (c) CV curves of the FZIB using AFLGE-30 and the coin battery using AFE-30 at −30 °C. (d) Rate capability of FZIB using AFLGE-30 at −30 °C. (e) Comparison of the FZIB using AFLGE-30 at various temperatures. (f) Long cycle performance at 100 mA/g of the FZIB using AFLGE-30 at various temperatures.

ethanol content at room temperature, which may be due to the lower dielectric constant (79.99 F/m for water and 25.02 F/m for ethanol at 20 °C) [48] and higher viscosity of ethanol (1.0 cP for water and 1.2 cP for ethanol at 20 °C) [49], contributing to an elevation in the resistance of the leather gel electrolyte (Fig. S8 in Supporting information). The charge/discharge performance of the FZIB using AFLGE-20, AFLGE-25, and AFLGE-30 at −30 °C are emphasized in Fig. 4b. The FZIB exhibits a superior specific capacity when using AFLGE-30, which is almost twice as much as when using AFLGE-20. The CV curve of the FZIB using AFLGE-30 shows the typical shape of a zinc-ion battery, with the same trend of the oxidation peak and reduction peak of the coin battery using AFE-30 (Fig. 4c). Subsequently, the rate capability of the FZIB using AFLGE-30 at −30 °C is tested in the range of 0.1, 0.2, 0.3, 0.4, 0.5 and 0.1 A/g, and the specific capacities of the battery cycled to the 10^{th} turn at each current density is 68.9, 37.4, 25.7, 15.8, 15.4, and 59.1 mAh/g, respectively (Fig. 4d). The specific capacity retention back to 0.1 A/g of the FZIB using AFLGE-30 can reach an excellent 85.8% compared to the initial capacity at the same current density. In addition, the battery shows more stable rate capability at −20 °C, and the specific capacity retention back to 0.1 A/g can reach 91.3% of the initial cycling at the same current density (Fig. S9 in Supporting information). Following this, continuous cycling tests are performed using one battery at 0.1 A/g in the range of 50 °C to −30 °C (Fig. 4e). As the temperature decreases, the specific capacity of the battery decreases which is similar to the decay of long cycling (Fig. 4f). Notably, the specific capacity of FZIB using AFLGE-30 is retained at only about 60% after 100 cycles at 50 °C, possibly because the layered structure of vanadium-based materials tends to collapse at higher temperatures. On the contrary, the long cycling stability of FZIB using AFLGE-30 is maintained at almost 100% at low temperatures (−20 °C, −30 °C). The enhanced suitability of the FZIB using the AFLGE-30 system at low temperatures is further illustrated.

Flexible batteries, which are core components in wearable electronic devices, may undergo a variety of complex stresses such as bending, twisting, and compression during use, impacting their structure and stability performance. It is conducive to improving their reliability and stability in practical applications in flexible electronic devices if the anti-destructive capacity of flexible zinc ion batteries is improved. FZIB using AFLGE-30 shows excellent flexibility in the bendability test, maintaining. 85.29% of its initial capacity after being bent for 500 times (Fig. 5a). In particular, even at fixed angles of 0°, 45°, 90°, 135°, and 180°, it retains over 92.12% of its initial capacity (Fig. 5b).

Moreover, the battery exhibits resilience against impacts, maintaining high capacity even under pressure and whacks compared to the original battery (Fig. 5c and Fig. S10 in Supporting information). The FZIB using AFLGE-30 can still light up the LED screen, even under continuous high pressure (Fig. S11 in Supporting information). It should be noted that polyimide film is used as the encapsulation material in the battery to avoid the flammability of AFLGE-30 due to the presence of ethanol. The flame retardancy of FZIB using AFLGE-30 is verified by placing it on an alcohol lamp for interval burning tests lasting 30 s, and the capacity loss is not significant (Fig. 5d).

In this work, a novel AFLGE-30 is successfully proposed. The high ionic conductivity and good mechanical properties of the gel electrolyte are achieved by utilizing bovine leather as the electrolyte matrix. The freezing point of the electrolyte is lowered by employing ethanol as a hydrogen bonding receptor in the hydrogel. At the same time, the desolventization ability of Zn^{2+} is weakened due to the modulation of the zinc anode passivation layer by introducing ethanol, resulting in a significant increase in the plating/stripping reversibility of Zn. The Zn//Zn symmetric battery life is up to 4100 h at room temperature. Even at low temperatures of −30 °C, full batteries maintain a specific capacity of about 70 mAh/g at a current density of 100 mA/g. In addition, the FZIB system has no significant capacity degradation after bending, pounding, and burning and still works normally at pressures up to 30 MPa. This study demonstrates that the addition of ethanol can improve the electrochemical performance of FZIBs at low temperatures as well as the protection of zinc anode, while the use of leather gel as the electrolyte can maintain high capacity and cycle life at low temperatures with good vandalism resistance.

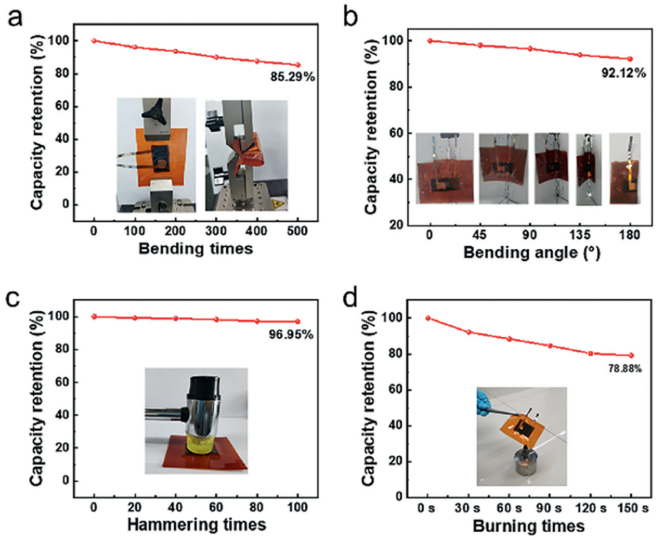

Fig. 5. Electrochemical properties of the FZIB using AFLGE-30 under different damages: (a) Repeated bending, (b) fixed-angle bending, (c) whacking, and (d) burning.

Declaration of competing interest

The authors declare that they have no known competing financial interests or personal relationships that could have appeared to influence the work reported in this paper.

CRediT authorship contribution statement

Mengxiao Yang: Conceptualization, Data curation, Formal analysis, Investigation, Methodology, Validation, Writing – original draft. **Haicheng Huang:** Data curation, Formal analysis. **Shiyi Shen:** Data curation, Investigation, Methodology. **Xinxin Liu:** Conceptualization, Data curation, Validation. **Mengyu Liu:** Data curation, Investigation, Methodology. **Jiahua Guo:** Investigation, Methodology, Validation. **Fenghui Yang:** Investigation, Methodology. **Baoli Zha:** Supervision, Writing – review & editing. **Jiansheng Wu:** Conceptualization, Funding acquisition, Project administration, Supervision, Writing – review & editing. **Sheng Li:** Conceptualization, Writing – review & editing. **Fengwei Huo:** Writing – review & editing.

Acknowledgment

The project is financially supported by the National Natural Science Foundation of China (Nos. 22075139 and 62288102).

Supplementary materials

Supplementary material associated with this article can be found, in the online version, at doi:10.1016/j.cclet.2024.109988.

References

[1] Z. Liang, M. Lu, H. Cheng, et al., Compos. Commun. 45 (2024) 101807.

[2] J. Li, C. Miao, J. Bian, et al., Chin. Chem. Lett. 34 (2023) 107996.
[3] L. Chen, H. Yue, Z. Zhang, et al., Chem. Eng. J. 455 (2023) 140679.
[4] Y. Zeng, J. Liang, J. Zheng, et al., Appl. Phys. Rev. 9 (2022) 021304.
[5] M. Yao, Z. Yuan, S. Li, et al., Adv. Mater. 33 (2021) e2008140.
[6] N. Wang, C. Sun, X. Liao, et al., Adv. Energy Mater. 10 (2020) 2002293.
[7] Q. Ding, X. Xu, Y. Yue, et al., ACS Appl. Mater. Interfaces 10 (2018) 27987–28002.
[8] H. Xia, G. Xu, X. Cao, et al., Adv. Mater. 35 (2023) e2301996.
[9] R. Ma, Z. Xu, X. Wang, Energy Environ. Mater. 6 (2023) e12464.
[10] P. Samanta, S. Ghosh, H. Kolya, et al., ACS Appl. Mater. Interfaces 14 (2022) 1138–1148.
[11] J. Wang, Y. Huang, B. Liu, et al., Energy Storage Mater. 41 (2021) 599–605.
[12] X. Li, D. Wang, F. Ran, Energy Storage Mater. 56 (2023) 351–393.
[13] F. Bu, Y. Gao, W. Zhao, et al., Angew. Chem. Int. Ed. 63 (2024) e202318496.
[14] S.J.R. Kelly, R. Weinkamer, L. Bertinetti, et al., J. Mech. Behav. Biomed. Mater. 90 (2019) 1–10.
[15] Z. Zhu, J. Zhu, Y. Chen, et al., Chin. Chem. Lett. 34 (2023) 107756.
[16] K.H. Shin, D. Ji, J.M. Park, et al., Adv. Funct. Mater. 34 (2024) 2309048.
[17] Y. Yuan, S.D. Pu, M.A. Perez-Osorio, et al., Adv. Mater. 36 (2024) 2307708.
[18] Y. Pu, C. Wang, J. Feng, et al., J. Power Sources 571 (2023) 233061.
[19] Y. Shi, R. Wang, S. Bi, et al., Adv. Funct. Mater. 33 (2023) 2214546.
[20] S. Huang, S. He, Y. Li, et al., Chem. Eng. J. 464 (2023) 142607.
[21] D. Zhang, Y. Liu, Y. Liu, et al., Adv. Mater. 33 (2021) e2104006.
[22] X. Han, H. Leng, Y. Qi, et al., Chem. Eng. J. 431 (2022) 133931.
[23] Y. Pan, Z. Liu, S. Liu, et al., Adv. Energy Mater. 13 (2023) 2203766.
[24] L. Yan, Q. Zhang, Z. Zhang, et al., J. Membr. Sci. 690 (2024) 122243.
[25] Y. Yan, S. Duan, B. Liu, et al., Adv. Mater. 35 (2023) e2211673.
[26] Q. Jian, T. Wang, J. Sun, et al., Chem. Eng. J. 466 (2023) 143189.
[27] B. Roy, U. Pal, M. Kar, et al., Curr. Opin. Green Sustain. Chem. 37 (2022) 100676.
[28] R. Wang, M. Yao, S. Huang, et al., Sci. China Mater. 65 (2022) 2189–2196.
[29] Q. Dou, S. Lei, D. Wang, et al., Energy Environ. Sci. 11 (2018) 3212–3219.
[30] Q. Nian, J. Wang, S. Liu, et al., Angew. Chem. Int. Ed. 58 (2019) 16994–16999.
[31] N. Chang, T. Li, R. Li, et al., Energy Environ. Sci. 13 (2020) 3527–3535.
[32] Y. Wu, Z. Zhu, D. Shen, et al., Energy Storage Mater. 45 (2022) 1084–1091.
[33] S. Huang, L. Hou, T. Li, et al., Adv. Mater. 34 (2022) 2110140.
[34] Y. Du, Y. Li, B.B. Xu, et al., Small 18 (2022) 2104640.
[35] H. Li, C. Han, Y. Huang, et al., Energy Environ. Sci. 11 (2018) 941–951.
[36] B.H. Lim, J.M. Kim, V.T. Nguyen, et al., Mater. Today Energy 33 (2023) 101263.
[37] B. Wang, J. Li, C. Hou, et al., ACS Appl. Mater. Interfaces 12 (2020) 46005–46014.
[38] C. You, R. Wu, X. Yuan, et al., Energy Environ. Sci. 16 (2023) 5096–5107.
[39] J. Cao, D. Zhang, X. Zhang, et al., Energy Environ. Sci. 15 (2022) 499–528.
[40] Q. Liu, Z. Yu, Q. Zhuang, et al., Adv. Mater. 35 (2023) e2300498.
[41] H. Meng, Q. Ran, T.Y. Dai, et al., Nano-Micro Lett. 14 (2022) 128.
[42] Y. Gao, Q. Cao, J. Pu, et al., Adv. Mater. 35 (2023) 2207573.
[43] T. Qiu, T. Wang, W. Tang, et al., Angew. Chem. Int. Ed. 62 (2023) e202312020.
[44] H.B. Chen, H. Meng, T.R. Zhang, et al., Angew. Chem. Int. Ed. 63 (2024) e202402327.
[45] W. Wang, S. Chen, X. Liao, et al., Nat. Commun. 14 (2023) 5443.
[46] Z. Zhao, J. Yin, J. Yin, et al., Energy Storage Mater. 55 (2023) 479–489.
[47] X. Li, J. Miao, F. Hu, et al., J. Mater. Chem. A 12 (2024) 968–978.
[48] M. Mohsen-Nia, H. Amiri, B. Jazi, J. Solution Chem. 39 (2010) 701–708.
[49] W. Rogula-Kozłowska, A. Mizerski, A. Walczak, et al., Matec. Web Conf. 247 (2018) 00064.